iScience

CellPress
OPEN ACCESS

Article

Inositol Pyrophosphate Metabolism Regulates Presynaptic Vesicle Cycling at Central Synapses

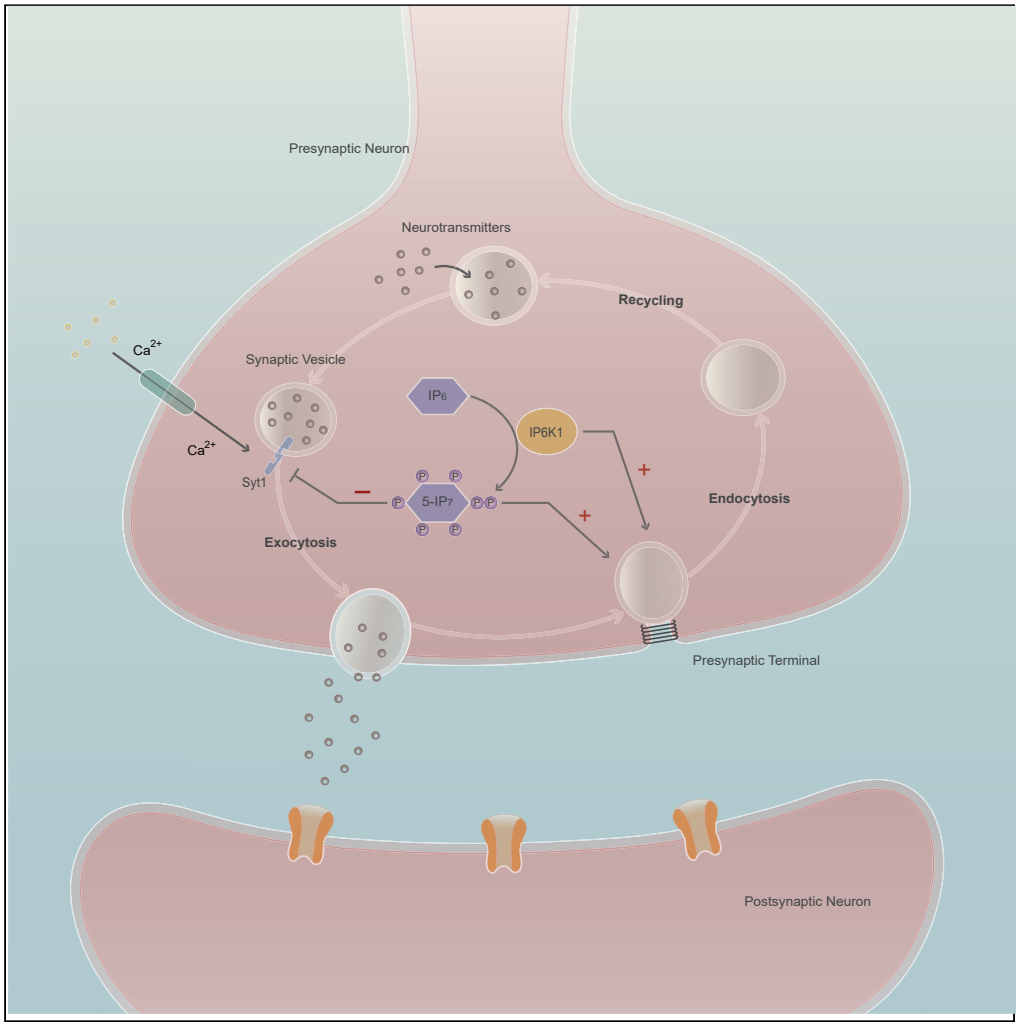

Seung Ju Park, Hoyong Park, Min-Gyu Kim, Seungjae Zhang, Seung Eun Park, Seyun Kim, ChiHye Chung

seyunkim@kaist.ac.kr (S.K.)
cchung@konkuk.ac.kr (C.C.)

HIGHLIGHTS

Excitatory synaptic vesicle release is increased in *Ip6k1*-KO hippocampal neurons

Wild-type IP6K1 restores presynaptic functions and plasticity of KO neurons

Catalytically inactive mutant IP6K1 fails to rescue defective presynaptic release

Synaptic endocytosis during exocytosis is severely impaired in *Ip6k1*-KO neurons

Park et al., iScience *23*, 101000
April 24, 2020
https://doi.org/10.1016/j.isci.2020.101000

iScience

CellPress
OPEN ACCESS

Article

Inositol Pyrophosphate Metabolism Regulates Presynaptic Vesicle Cycling at Central Synapses

Seung Ju Park,[1,4] Hoyong Park,[2,4] Min-Gyu Kim,[1,4] Seungjae Zhang,[2] Seung Eun Park,[1] Seyun Kim,[1,3,5,*] and ChiHye Chung[2,*]

SUMMARY

The coordination of synaptic vesicle exocytosis and endocytosis supports neurotransmitter release from presynaptic terminals. Although inositol pyrophosphates, such as 5-diphosphoinositol pentakisphosphate (5-IP$_7$), are versatile signaling metabolites in many biological events, physiological actions of 5-IP$_7$ on synaptic membrane vesicle trafficking remain unclear. Here, we investigated the role of 5-IP$_7$ in synaptic transmission in hippocampal brain slices from inositol hexakisphosphate kinase 1 (*Ip6k1*)-knockout mice. We found that presynaptic release probability was significantly increased in *Ip6k1*-knockout neurons, implying enhanced activity-dependent synaptic vesicle exocytosis. Expression of wild-type but not catalytically inactive IP6K1 in the *Ip6k1*-knockout hippocampus restored the altered presynaptic release probability. Moreover, *Ip6k1*-knockout neurons were insensitive to folimycin, a vacuolar ATPase inhibitor, and dynasore, a dynamin inhibitor, suggesting marked impairment in synaptic endocytosis during exocytosis. Our findings collectively establish that IP6K1 and its product, 5-IP$_7$, act as key physiological determinants for inhibition of presynaptic vesicle exocytosis and stimulation of endocytosis at central synapses.

INTRODUCTION

Inositol phosphates (IPs), found in organisms ranging from yeast to mammals, act as molecular messengers that mediate diverse cellular functions, including growth and metabolism (Chakraborty et al., 2011; Hatch and York, 2010; Shears, 2015; Wilson et al., 2013). Inositol 1,4,5-trisphosphate (IP$_3$), perhaps the best-known IP metabolite, triggers increases in cytosolic Ca^{2+} levels through direct binding and activation of IP$_3$-gated Ca^{2+} channels in the ER(Irvine and Schell, 2001). The identification of IP kinases and phosphatases led to the discovery of higher inositol polyphosphates containing multiple phosphates, such as inositol hexakisphosphate (IP$_6$) (Seeds et al., 2007). In mammals, the most extensively characterized inositol pyrophosphate is 5-diphosphoinositol pentakisphosphate (5-PP-[1,2,3,4,6]IP$_5$), designated 5-IP$_7$, which is synthesized by phosphorylation of fully phosphorylated six-carbon inositol IP$_6$ at position 5 (Chakraborty et al., 2011; Park et al., 2018).

The biosynthesis of 5-IP$_7$ is catalyzed by a family of three inositol hexakisphosphate kinases (IP6Ks) (Saiardi et al., 1999). Among these, IP6K1 is highly expressed in the brain (Saiardi et al., 1999); however, its neuronal functions remain poorly understood. As shown in non-neuronal cells (e.g., hepatocytes), the IP6K1 product, 5-IP$_7$, inhibits brain Akt activity (Chakraborty et al., 2014). Moreover, IP6K1 can directly bind and stimulate glycogen synthase kinase 3 (GSK3) in a non-catalytic manner (Chakraborty et al., 2014). *Ip6k1*-null mice exhibit reduced GSK3 activity and thus manifest behavioral defects such as reduced locomotive responsiveness to amphetamine as well as impaired social interactions (Chakraborty et al., 2014). It was also suggested that IP6K1 catalytic activity controls α-actinin and focal adhesion kinase, based on the observation that deletion of IP6K1 leads to retarded neuronal migration in the cerebral cortex (Fu et al., 2017).

Synaptic vesicle cycling is a fundamental process in cell-to-cell communication that underlies virtually all neural activities, as exemplified by neurotransmitter release (Schweizer and Ryan, 2006; Südhof, 2004). Since the early 1990s, IPs have been highlighted for their role as endogenous signaling metabolites that influence synaptic vesicle cycling (Llinás et al., 1994; Yang et al., 2012). 5-IP$_7$ was shown to exert potent

[1]Department of Biological Sciences, Korea Advanced Institute of Science and Technology (KAIST), Daejeon 34141, Korea

[2]Department of Biological Sciences, Konkuk University, Seoul 05029, Korea

[3]KAIST Institute for the BioCentury, KAIST, Daejeon 34141, Korea

[4]These authors contributed equally

[5]Lead Contact

*Correspondence: seyunkim@kaist.ac.kr (S.K.), cchung@konkuk.ac.kr (-g.C.)

https://doi.org/10.1016/j.isci.2020.101000

inhibitory activity toward synaptic vesicle exocytosis through direct inhibition of synaptotagmin 1 (Syt1), a Ca^{2+} sensor essential for synaptic membrane fusion (Lee et al., 2016). In PC12 cells, increasing 5-IP_7 levels by overexpressing IP6K1 suppresses depolarization-induced neurotransmitter release, whereas decreasing 5-IP_7 concentrations by IP6K1 knockdown leads to enhanced exocytosis. IP6K1 knockdown in cultured hippocampal neurons augments action-potential-driven synaptic vesicle exocytosis (Lee et al., 2016). By contrast, IP6K1 was previously found to non-catalytically stimulate dopamine release in PC12 cells through direct protein-protein interaction with GRAB, a guanine nucleotide exchange factor for Rab3A (Luo et al., 2001). In non-neuronal cells, IP6K1 and 5-IP_7 have also been implicated in the fine control of endocytosis. Budding yeast devoid of KCS1, the *S. cerevisiae* homolog of mammalian IP6K1, exhibits defective endocytic membrane trafficking (Saiardi et al., 2002). Nonetheless, physiological neuronal functions of 5-IP_7 metabolism in the regulation of synaptic vesicle cycling have remained largely elusive.

In this study, we electrophysiologically investigated synaptic vesicle cycling in *Ip6k1*-knockout (KO) mice. We found that the loss of IP6K1 enhanced presynaptic release probability and deregulated synaptic vesicle endocytosis at active hippocampal synapses, thereby establishing physiological roles of IP6K1 and inositol pyrophosphates in the fine control of synaptic vesicle exocytosis as well as endocytic recycling.

RESULTS

Generation of IP6K1-KO Mice

To investigate physiological roles of IP6K1 in the control of synaptic vesicle trafficking, we employed the CRISPR/Cas9 system to generate mice with a targeted deletion of IP6K1. To ensure complete disruption of functional proteins, we chose target sites near the translational start ATG codon in exon 2 of mouse *Ip6k1* (Figure 1A). The gRNA-Cas9 system induced the expected mutation in the targeting site, and the mutated allele included a 73-bp deletion that resulted in a frameshift and premature termination (Figure 1B). Immunoblotting of brain extracts using IP6K1-specific antibodies confirmed the absence of IP6K1 protein in homozygous *Ip6k1* exon 2-deleted (IP6K1-KO) mice (Figure 1C). We next examined whether IP6K1 catalytic activity was lost in IP6K1-KO mice by measuring IP_7 levels from IP6K1-KO and wild-type (WT) mice. Similar to a previous report by Chakraborty et al. using IP6K1-KO mice harboring a deletion of exon 6 corresponding to the kinase domain (Chakraborty et al., 2010), we found that IP_7 levels in primary hippocampal neurons (Figure 1D) and hepatocytes (Figure S1A) from our IP6K1-KO mice were markedly reduced (~60% and ~50%, respectively) and insulin-stimulated Akt activation was enhanced in IP6K1-KO hepatocytes (Figure S1B), confirming the successful generation of IP6K1-KO mice through targeting of the ATG start codon. Using Nissl staining to analyze brain architecture, we found that brain structure was normal in both 5-week-old IP6K1-KO mice (Figure 1E) and 8-week-old IP6K1-KO mice (Figure S2A). An analysis of the anatomy of the hippocampus, the primary target of our electrophysiological analyses, showed that hippocampal formation was normal in young (5-week-old, Figure 1F) and adult (8-week-old, Figure S2B) IP6K1-KO mouse brains, confirming that loss of IP6K1 does not affect hippocampal development. Expression of two other IP6K isoforms (IP6K2 and IP6K3) was not altered by the loss of IP6K1 (Figure S3). IP6K1 was detected in synaptic fractions, including crude synaptosomes, synaptic membranes, and synaptic vesicle fractions of the mouse brain (Figure S4), providing evidence for the synaptic presence of IP6K1. We further checked that IP6K1-KO brain expresses normal amounts of synaptic proteins, including synaptotagmin, dynamin, presynaptic vesicular glutamate transporters, AP2, v-ATPase, phosphatidylinositol 4-phosphate 5-kinase (Figure S5).

Enhanced Excitatory Synaptic Vesicle Release of IP6K1-KO Hippocampal Neurons

To assess the functional effect of IP6K1 deletion on synaptic transmission *ex vivo*, we recorded excitatory postsynaptic currents (EPSCs) evoked by electrical stimulation of Schaffer collateral pathways 100 times at various frequencies (10, 20, and 50 Hz) in acute hippocampal brain slices from IP6K1-KO and WT mice. A plot of normalized evoked EPSC (eEPSC) amplitudes against time at each frequency revealed short-term synaptic plasticity in hippocampi from both genotypes. Interestingly, the rate of short-term synaptic facilitation was greater in WT mice than IP6K1-KO mice at stimulation frequencies of 20 and 50 Hz stimulation ($p > 0.11$ for 10 Hz; $p < 0.05$ for 20 Hz, $p < 0.001$ for 50 Hz) (Figures 2A and 2B). Given that the balance between residual Ca^{2+} and initial release probability determines short-term synaptic plasticity, presynaptic release probability is likely to be increased in IP6K1-KO mice. Consistent with this, paired-pulse ratio (PPR) was significantly decreased upon higher frequency stimulation ($F_{(1,68)} = 20.504$, $p < 0.0001$ for genotype; $F_{(2,68)} = 3.728$, $p < 0.05$ for frequency) (Figure 2C). Besides the PPR, we calculated the release probability by the amplitude of first eEPSC divided by the size of readily releasable synaptic vesicle pool (RRP). RRP size was estimated by using back extrapolation of cumulative eEPSC charge transfer during

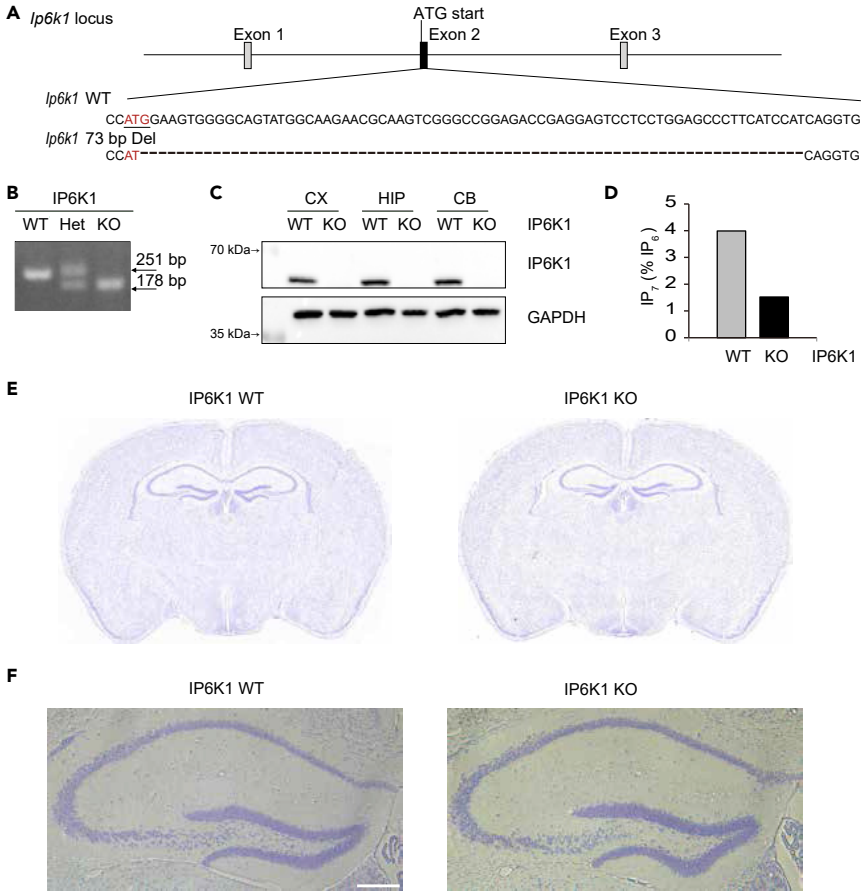

Figure 1. Generation and Characterization of IP6K1-KO Mice

(A) Schematic depiction of the strategy for *Ip6k1* gene disruption. Sequences of *Ip6k1* alleles from IP6K1-KO mice generated by the CRISPR/Cas9 system are displayed. The start codon (ATG) underlined in green is disrupted in IP6K1-KO mice. A 73-bp, out-of-frame deletion within *Ip6k1* exon 2 in IP6K1-KO mice is indicated by dashes.

(B) Representative PCR genotyping results for *Ip6k1* WT, homozygous (KO), and heterozygous (Het) mice.

(C) Immunoblot analysis shows depletion of IP6K1 protein from brain tissues of IP6K1-KO mice. CX, cortex; CB, cerebellum; HIP, hippocampus.

(D) WT and IP6K1-KO hippocampal neurons were cultured and labeled with [^{3}H]myo-inositol, and intracellular inositol phosphates were resolved by HPLC. Quantification indicates ~60% reduction of IP_7 in IP6K1-KO hippocampal neurons.

(E and F) Nissl staining shows normal brain structures of 5-week-old, IP6K1-KO mice (E). Representative images of hippocampal regions are shown in (F). Scale bar, 200 μm.

sustained stimulus (20 Hz) (Lou et al., 2012; Macia et al., 2006; Thanawala and Regehr, 2013). Consistent with our observations with release probability measured by PPR, the calculated release probability was significantly increased in IP6K1-KO mice (Figure 2D, $p < 0.05$). The current findings thus suggest that IP6K1 may be one of the physiological regulators involved in clamping synaptic exocytosis and show that the impact of IP6K1 deletion on short-term synaptic plasticity is activity dependent.

We further found that the frequency and amplitude of miniature EPSCs (mEPSCs) were not different between IP6K1-KO and WT mice ($p > 0.53$ for frequency; $p > 0.30$ for amplitude) (Figure 2E), suggesting that spontaneous synaptic transmission is minimally affected by deletion of IP6K1.

To examine whether deficiency of IP6K1 leads to postsynaptic changes, we measured the relative contribution of two major glutamate receptors, the α-amino-3-hydroxy-5-methyl-4-isoxazolepropionic acid receptor (AMPAR) and N-methyl-D-aspartate receptor (NMDAR), on excitatory currents by recording eEPSCs at −60 mV and +40 mV and calculating the ratio of AMPAR- and NMDAR-mediated currents (A/N ratio). There was no difference in the A/N ratio between IP6K1-KO and WT mice ($p > 0.69$, Figure 2F).

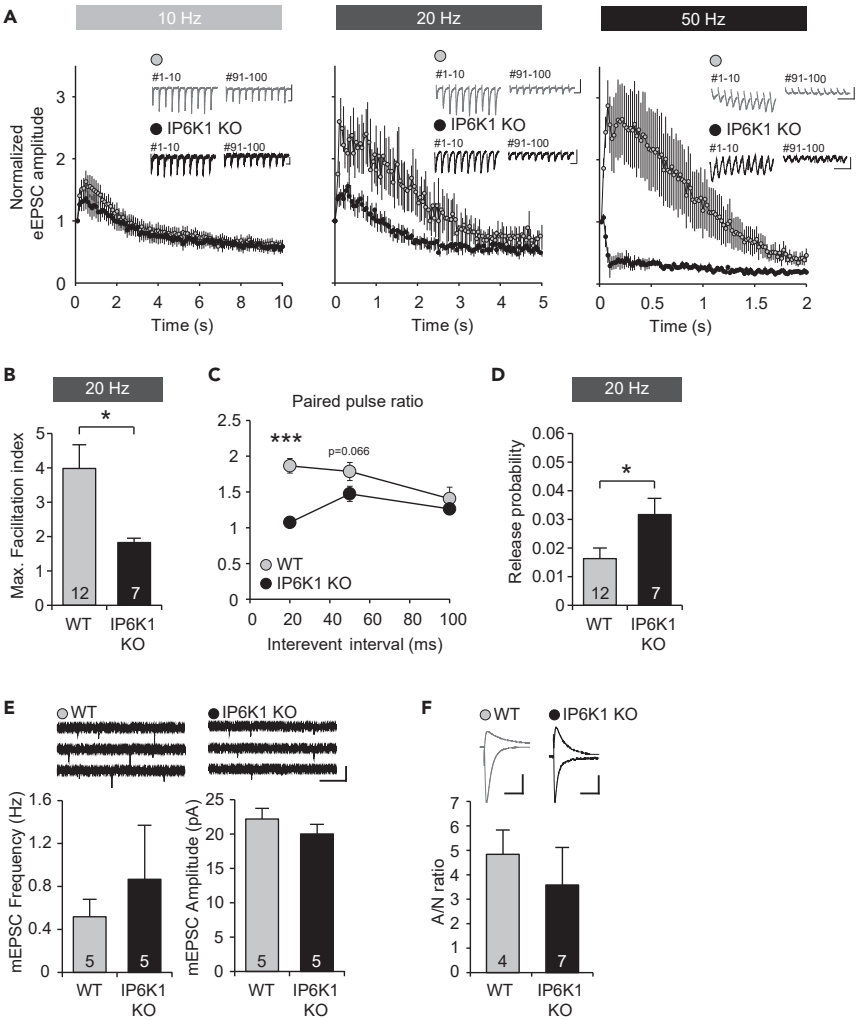

Figure 2. Evoked Excitatory Presynaptic Vesicle Release is Enhanced in Hippocampal Neurons from IP6K1-KO Mice

(A) Normalized eEPSC amplitudes in hippocampal neurons from IP6K1-KO mice decreased markedly faster than those from WT mice following 100 pulses of 20 Hz or 50 Hz stimulation, but not 10 Hz stimulation (10 Hz stimulation, n = 7–11, minimum $p > 0.11$; 20 Hz stimulation, n = 7–12, *$p < 0.05$ for stimuli 3-4; 50 Hz stimulation, n = 4–9, *$p < 0.05$ for stimuli 15-31, **$p < 0.01$ for stimuli 8-14, ***$p < 0.001$ for stimuli 2-4). Scale bars for representative traces: 100 pA and 50 ms.

(B) Maximum facilitation index following 20 Hz stimulation was significantly decreased in IP6K1-KO mice (*$p < 0.05$).

(C) PPR was significantly decreased in an activity-dependent manner (two-way ANOVA analysis, $F_{(1,49)} = 20.504$, ***$p < 0.001$ for genotype; $F_{(2,49)} = 3.728$, *$p < 0.05$ for frequency).

(D) Calculated release probability was enhanced in IP6K-KO mice (*$p < 0.05$).

(E) Frequencies and amplitudes of mEPSCs were not altered in IP6K1-KO mice (n = 5 for each group; $p > 0.53$ for frequency; $p > 0.30$ for amplitude). Scale bars for representative traces: 50 pA and 1 s.

(F) There was no alteration in A/N ratio (n = 4–7, $p > 0.69$). Scale bars for representative traces: 50 pA and 50 ms.

Presynaptic Release Probability Alteration in Hippocampal Inhibitory Synapses in IP6K1-KO Mice

Next, we measured evoked inhibitory postsynaptic currents (eIPSCs) to determine the role of IP6K1 on synaptic vesicle recycling in inhibitory synapses. PPRs of eIPSCs altered compared between genotypes ($p < 0.05$ for 10 Hz; $p > 0.5$ for 20 Hz) (Figures S6A and S6B). PPRs in GABAergic synapses were significantly increased in IP6K1-KO mice, suggesting decreased synaptic vesicle releases. These observations indicate that deletion of IP6K1 induces alteration of synaptic transmission in both excitatory and inhibitory synapses, although the level of changes were a lot smaller in inhibitory synapses, suggesting that the action of IP6K1 may differ depending on the availability of its interacting partners at different types of synapses.

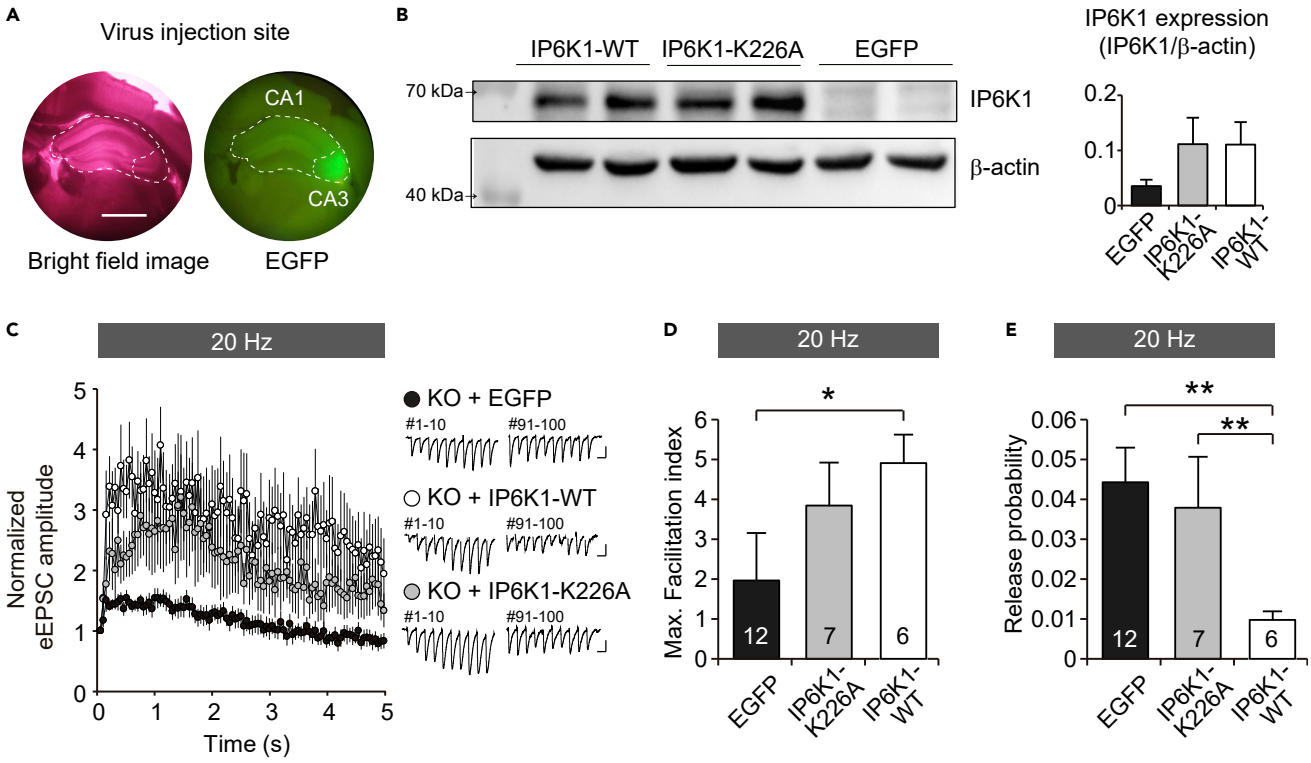

Figure 3. Hippocampus-specific Expression of IP6K1 Restored Synaptic Changes Observed in IP6K1-KO Mice

(A) Representative images for virus injection site. The bright field image of hippocampus containing brain slice (left). EGFP-labeled hippocampal CA3 regions of IP6K1-KO mice by AAV-WT-IP6K1 or IP6K1-K/A and AAV-EGFP control virus injection (right). Scale bar, 1 mm.

(B) Immunoblot analysis shows restoration of IP6K1 protein from hippocampal tissues of AAV injected IP6K1-KO mice (n = 2–3).

(C) Normalized eEPSC amplitudes from IP6K1-KO mice after expression of IP6K1 (IP6K1-WT) or catalytically inactive form of IP6K1 (IP6K1-K226A). Facilitation of eEPSC amplitude was significantly enhanced in IP6K1-WT-injected IP6K1-KO mice following 100 pulses of 20 Hz stimulation. IP6K1-K226A-expressing mice showed moderate facilitation of eEPSC (IP6K-WT versus EGFP, n = 6–12, *p < 0.05 for stimuli 3, **p < 0.01 for stimuli 28-100, ***p < 0.001 for stimuli 4-27; IP6K1-K226A versus EGFP, n = 7–12, *p < 0.05 for stimuli 4-99). Scale bars for representative traces: 100 pA and 50 ms.

(D) Maximum facilitation index following 20 Hz stimulation was significantly increased in IP6K1-WT-expressing KO mice (One-way ANOVA analysis, n = 6–12, $F_{(2,22)}$ = 3.547, *p < 0.05).

(E) Calculated release probability was decreased in IP6K1-WT-expressing KO mice (one-way ANOVA analysis n = 6–12, $F_{(2,22)}$ = 6.534, **p < 0.01), whereas no significant changes were observed between EGFP-injected and IP6K1-K226A-injected KO mice.

Restoration of Presynaptic Release Probability and Short-Term Plasticity by Expression of WT-IP6K1 in IP6K1-KO Mice

To investigate whether the local expression of IP6K1 in the hippocampus restores short-term synaptic plasticity as shown in WT hippocampus, we virally delivered AAV-IP6K1-WT or AAV-EGFP in the hippocampal CA3 regions of IP6K1-KO mice. After four weeks of injection, we observed ample amount of IP6K1 expression in the whole hippocampus obtained from IP6K1-KO mice (Figures 3A and 3B). Upon sustained electrical stimulus (20 Hz, 100 times), IP6K1-WT-injected KO mice showed restored short-term plasticity and presynaptic release probability in Schaffer collateral pathway (Figures 3C–3E, $F_{(2,22)}$ = 3.547, p < 0.05 for facilitation index, $F_{(2,22)}$ = 6.534, p < 0.01 for release probability).

In order to examine whether the catalytic activity of IP6K1 is required for IP6K1-dependent synaptic changes, we generated catalytically inactive IP6K1 harboring a single K226A point mutation (Lee et al., 2016). Importantly, enhanced presynaptic release probability seems to remain high even after IP6K1-K226A expression in IP6K1 KO mice (Bonferroni post hoc., EGFP KO versus IP6K1-K226A-injected KO, p > 0.09; IP6K1-WT versus IP6K1-K226A-injected KO, p < 0.01), validating that IP6K1's product, 5-IP_7, plays a role in suppressing presynaptic exocytosis. Interestingly, IP6K1-K226A-injected KO mice showed partially restored short-term plasticity (Bonferroni post hoc., EGFP KO versus IP6K1-K226A-injected KO, p > 0.9; IP6K1-WT versus IP6K1-K226A-injected KO, p > 0.2). Our rescue experiments thus revealed that IP6K1

regulates both synaptic vesicle release probability and short term facilitation; however, the catalytic activity of IP6K1 is required for regulation of the release probability but not for short-term facilitation.

Suppressed Synaptic Vesicle Resupply after Vesicle Exhaustion in IP6K1-KO Neurons

To further investigate the impact of IP6K1 deletion on synaptic vesicle trafficking, we challenged presynaptic terminals of the hippocampus with excessive electrical stimulation (20 Hz for 15 s), followed by 1-Hz stimulation. Trains of stimulation at 20 Hz resulted in successful temporary depletion of available vesicles in both WT and IP6K1-KO mice ($p > 0.22$; Figure 4A). After synaptic vesicle exhaustion, we measured eEPSC amplitude during 1-Hz stimulations for 3 min to allow restoration of synaptic responses. In WT mice, synaptic responses recovered to ~70% of their initial amplitude in 50 s and fully recovered at the end of 1-Hz trains ($p > 0.99$; Figures 4A and 4C). In the case of IP6K1-KO hippocampal slices, however, synaptic responses recovered to ~40% of their initial amplitude in 50 s and ~60% at the end of 1-Hz trains ($p < 0.01$; Figures 4A and 4C), indicating that the magnitude of restored responses was significantly reduced in IP6K1-KO mice ($p < 0.05$; Figure 4D). These observations show that IP6K1 deletion limits synaptic vesicle resupply to the recycling pool of synaptic vesicles following intensive challenge. This was not attributable to differences in initial eEPSC amplitudes, because the averaged initial eEPSC amplitudes were not significantly different between genotypes ($p > 0.19$; Figure 4B). To quantitatively compare rates of synaptic depression and synaptic recovery, we fitted normalized graphs for the falling phase and rising phase to a single exponential function. Time constants of the falling phase ($p > 0.68$) and rising phase ($p > 0.32$) were not different between genotypes (Figure 4E), suggesting that synaptic vesicles cannot be fully restored after synaptic vesicle exhaustion in the context of IP6K1 deletion.

Impaired Vesicle Reuse During Exocytosis in IP6K1-KO Neurons

Previous studies using *in vitro* assays have reported that IPs such as IP_6 bind and functionally interrupt clathrin assembly proteins (APs), such as AP-2 and AP-3, which are instrumental in vesicle endocytosis (Norris et al., 1995; Voglmaier et al., 1992; Ye et al., 1995). IP_6-regulated downstream signaling events were also found to control synaptic vesicle proteins required for endocytosis (Hilton et al., 2001). In pancreatic beta cells, IP_6 appears to promote dynamin-mediated endocytosis in association with insulin exocytosis (Hoy et al., 2002). Does IP6K1 deficiency have any impact on synaptic vesicle endocytosis per se at central synapses? To address this question, we employed an additional pharmacological manipulation to isolate exocytosis and endocytosis during recordings (Figure 5A). Folimycin is a vacuolar-ATPase inhibitor that decreases synaptic output by interrupting the neurotransmitter refilling step (Sankaranarayanan and Ryan, 2001). To limit synaptic vesicle reuse, we recorded evoked excitatory responses in the absence or presence of folimycin while stimulating at 20 Hz. In WT animals, treatment of hippocampal slices with folimycin (80 nM for 10 min) caused use-dependent synaptic depression of eEPSCs compared with that in pre-folimycin treatment controls ($p < 0.01$; Figure 5B), as reported previously (Ertunc et al., 2007). The difference in eEPSC amplitudes before and after folimycin treatment reflects the amount of synaptic vesicle endocytosis that occurred during stimulation, supporting previous observations that recycled vesicles are rapidly recruited for synaptic transmission (Ertunc et al., 2007). However, folimycin treatment in IP6K1-KO mice did not reveal any involvement of endocytic components during 20-Hz stimulation, suggesting that endocytosis during exocytosis might be impaired in these mice ($p < 0.05$; Figure 5B). There were no alterations in initial eEPSC amplitudes between before and after folimycin treatment ($p > 0.08$; Figure 5C).

To directly examine the impact of IP6K1 in endocytosis, we employed a small molecule dynamin inhibitor, called dynasore (Macia et al., 2006; Newton et al., 2006). Incubation with 80 μM dynasore induced notable use-dependent short-term depression in WT ($p < 0.05$; Figure 5D), whereas no difference in IP6K1-KO synapses ($p > 0.1$; Figure 5D), suggesting that the acute blockade of dynamin function has limited impact in synaptic transmission during high challenges in the absence of IP6K1 as if dynamin has not been working in IP6K1-KO synapses. Taken together, our data suggest that IP6K1 and 5-IP_7 metabolism are likely to be involved in regulation of synaptic vesicle endocytosis and coupling between exo- and endocytosis.

DISCUSSION

Tight coupling between exocytosis and endocytosis is critical for coordinating synaptic transmission at central synapses. It has been decades since inositol poly- and pyrophosphates were suggested as key metabolites in the regulation of synaptic vesicle control (Wenk and De Camilli, 2004). Among these IPs, 5-IP_7 was recently proposed as the most potent in suppressing synaptic vesicle exocytosis, but these conclusions

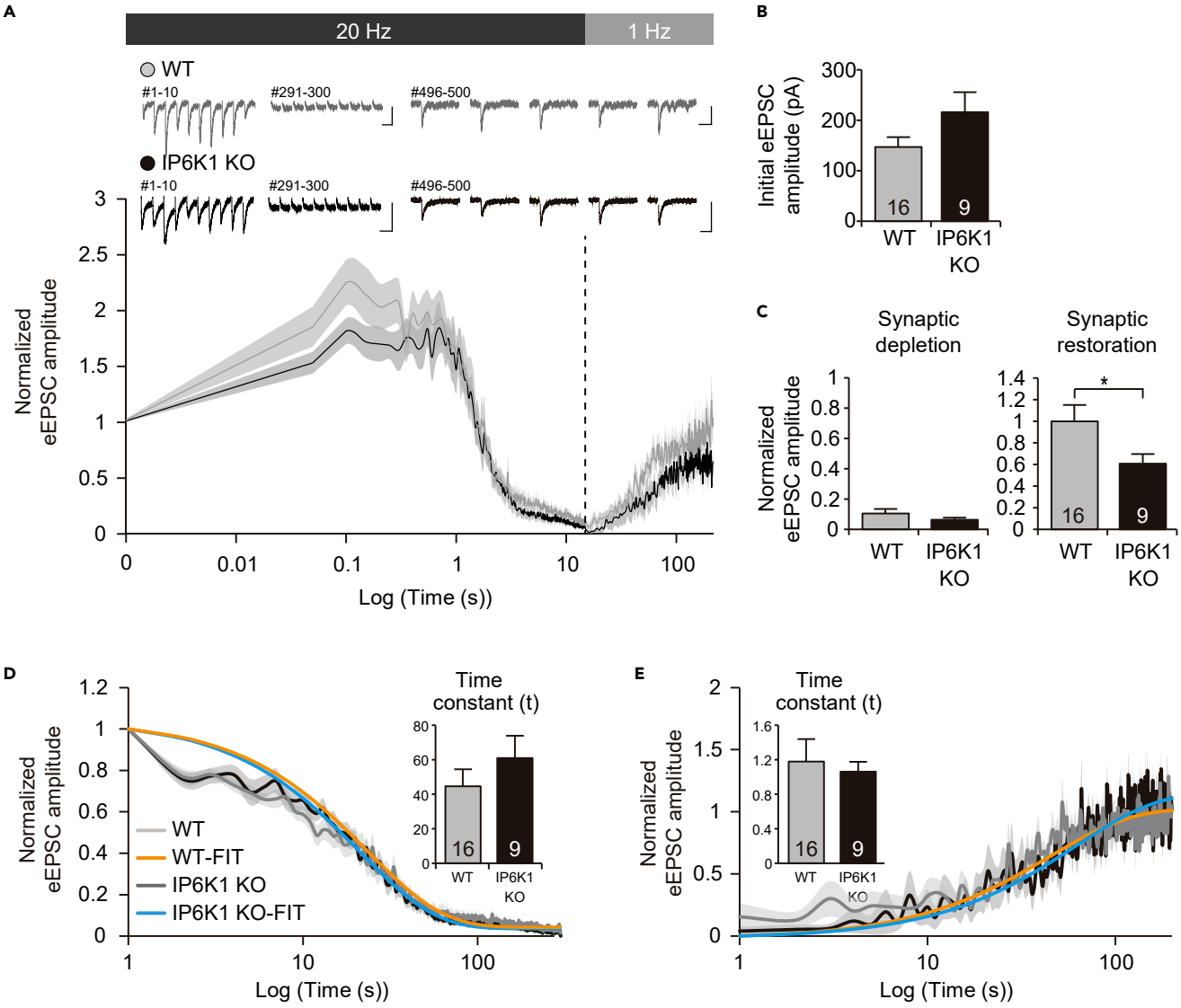

Figure 4. Synaptic Vesicle Resupply after Exhaustion is Suppressed in Hippocampal Neurons from IP6K1-KO Mice

(A) Normalized eEPSC amplitudes were substantially depressed during 20-Hz stimulation and gradually increased during 1-Hz stimulation (n = 9–16).

(B) Average initial eEPSC amplitudes were comparable between genotypes ($p > 0.19$).

(C) The magnitude of eEPSC depression was comparable in IP6K1-KO (n = 16) and WT (n = 9) mice ($p > 0.22$).

(D) The magnitude of eEPSC restoration was significantly reduced in IP6K1-KO mice (*$p < 0.05$).

(E) Time constants (τ) of synaptic vesicle exhaustion and resupply were not different between IP6K1-KO and WT mice ($p > 0.68$ for τ during exhaustion; $p > 0.32$ for τ during resupply). Representative fits to single-exponential functions for WT mice (orange) and IP6K1-KO mice (blue) are shown for synaptic vesicle exhaustion (WT, τ =23.51; KO, τ =21.17) and synaptic vesicle resupply (WT, τ =44.52; KO, τ =60.97). Scale bars for representative traces: 100 pA and 50 ms.

have been drawn from experiments using cell lines or primary cultures. To define this important issue at a physiological level, we took advantage of mice genetically lacking *Ip6k1* and employed electrophysiological approaches to probe the function of IP6K1 in synaptic vesicle recycling in acute hippocampal slices. Our principle findings can be summarized as follows: (1) Measurements of evoked EPSCs revealed that deletion of IP6K1 increased presynaptic release probability, suggesting enhanced excitatory synaptic vesicle fusion. (2) Short-term facilitation was decreased in IP6K1-KO neurons. (3) WT IP6K1, but not catalytically inactive mutant IP6K1, successfully restored a phenotype of presynaptic release probability in IP6K1-KO neurons. (4) Both WT and catalytically inactive IP6K1 recovered short-term facilitation of IP6K1-KO neurons. (5) The IP6K1-KO hippocampus failed to respond to folimycin and dynasore, indicating that endocytosis during exocytosis is severely impaired in IP6K1-KO mice. Collectively, these findings

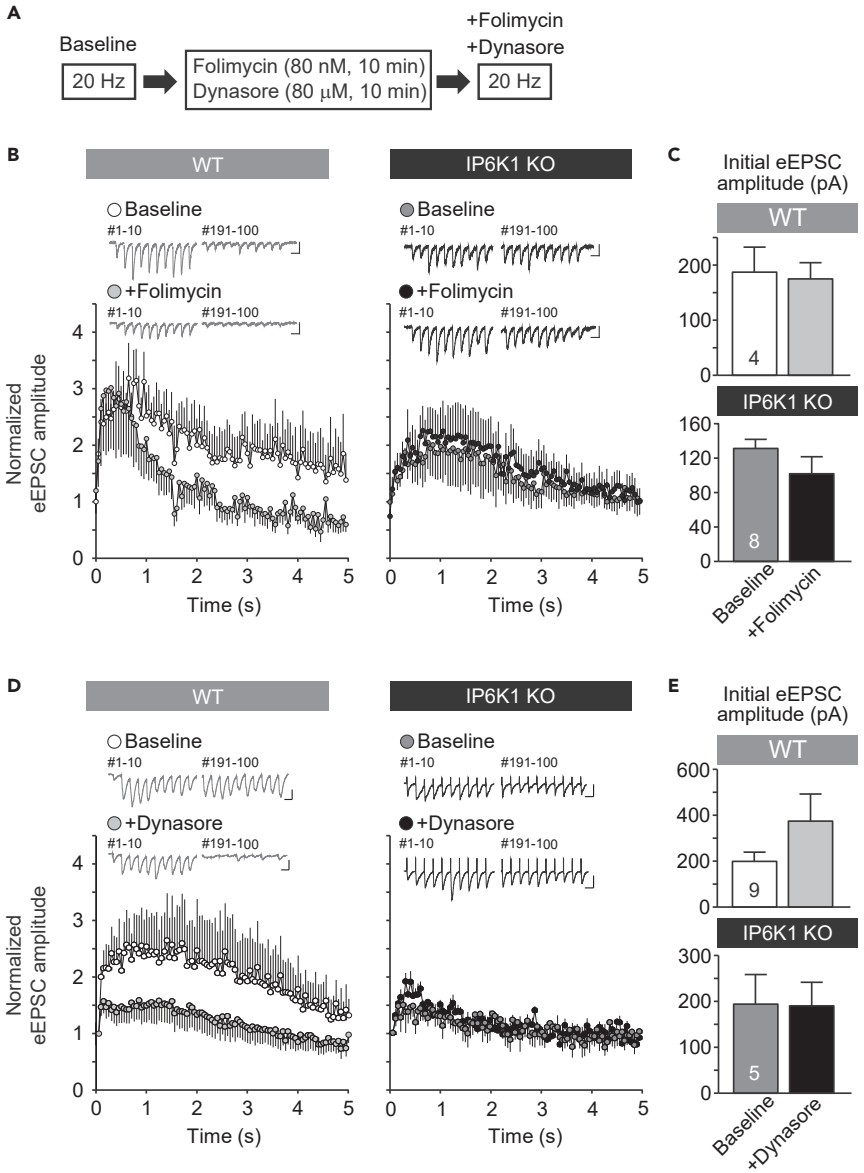

Figure 5. Synaptic Vesicle Endocytosis and Reuse are Impaired in Hippocampal Neurons from IP6K1-KO Mice

(A and B) (A) Experimental scheme for the vesicle-reuse test. (B) After folimycin treatment (80 nM, 10 min), the rate of eEPSC depression from hippocampal neurons during 20 Hz stimulation in WT mice was significantly faster than that before treatment ($n = 4$, $^*p < 0.05$ for stimuli 15-41 and 50-78). There was no difference in eEPSC depression rate between before and after folimycin treatment in IP6K1-KO mice ($n = 8$, minimum $p > 0.08$). Scale bars for representative traces: 100 pA and 50 ms.

(C) Initial eEPSC amplitudes were not different in WT or IP6K1-KO groups ($p > 0.63$ for WT, $p > 0.13$ for IP6K1-KO).

(D) Dynasore treatment (80 μM, 10 min) expedite the synaptic depression during 20-Hz stimulation ($n = 5$–9, $^*p < 0.05$ for stimuli 6-20). Dynasore has minimal effect in IP6K1-KO synapses ($p > 0.1$).

(E) Initial amplitudes of eEPSCs were comparable between WT and IP6K1-KO groups ($p > 0.15$ for WT, $p > 0.84$ for IP6K1-KO).

reveal physiological roles of 5-IP_7 metabolism in controlling synaptic vesicle exocytosis and endocytosis, as well as their coupling.

A possible mechanistic explanation for the selective enhancement of synaptic vesicle exocytosis in excitatory synaptic function in IP6K1-KO mice is interaction between the IP6K1 product, 5-IP_7, and Syt1, a

Ca^{2+} sensor enriched in excitatory synapses (Fernandez-Chacon et al., 2001; Geppert et al., 1994; Rizo and Rosenmund, 2008). Syt1 function can be potently suppressed by its high-affinity ligand, 5-IP_7, which interacts with the polybasic C2B domain of Syt1 to reduce synaptic vesicle fusion (Lee et al., 2016). Cultured hippocampal neurons harboring a mutant form of Syt1 with a point mutation in the Ca^{2+}-sensing domain exhibit impaired neurotransmitter release and abnormally facilitated synaptic responses to successive stimulation (Fernandez-Chacon et al., 2001). Taken together, these observations suggest that depletion of the Syt1 inhibitor 5-IP_7 by IP6K1-KO contributes to the facilitation of synaptic vesicle fusion.

Interestingly, we found IP6K1 regulates release probability and short-term facilitation in two distinct mechanisms. When we fully restored IP6K1 in KO hippocampus, both release probability and short-term facilitation were recovered to the levels of WT. However, expression of catalytically inactive form of IP6K1 failed to rescue presynaptic release probability in the IP6K1-KO neurons, clearly demonstrating that IP6K1's product, 5-IP_7, is the key factor in the control of presynaptic vesicle exocytosis (Figure 3). Introduction of catalytically inactive mutant IP6K1 could restore short-term facilitation to the levels comparable to WT (Figure 3), suggesting a non-catalytic action of IP6K1 enzyme in the regulation of presynaptic events.

IP6K1 is known to directly interact with GRAB, a GDP-GTP exchange factor for a subset of Rab GTPases, including Rab3 and Rab8, and this interaction does not require catalytic activity (Guo et al., 2013; Luo et al., 2001). GSK3 is also known as activated by non-catalytic interactions between IP6K1 and GSK3 (Chakraborty et al., 2010, 2014). Therefore, IP6K1 appears to interact with synaptic proteins regardless of its catalytic activity, which may be sufficient to restore short-term facilitation but not release probability. Several studies suggest the role of GSK3 and Rab GTPase in short-term synaptic plasticity. GSK3 is known to directly phosphorylate and modulate dynamin (Clayton et al., 2010), a GTPase required for synaptic vesicle fission events. Inhibition of dynamin phosphorylation enhances short-term synaptic depression upon high-frequency stimulation (Fà et al., 2014). Moreover, Rab3A is involved in short-term synaptic facilitation. Mutation or deletion of Rab3A protein was shown to enhance synaptic facilitation upon repetitive stimulation (Doussau et al., 1998; Geppert et al., 1997; Schluter et al., 2006). These studies suggest that non-catalytic interaction of IP6K1 with GSK3 or GRAB may mediate short-term synaptic facilitation in the hippocampus.

Since the first report by Saiardi et al. (Saiardi et al., 2002) that budding yeast lacking inositol pyrophosphates by the deletion of KCS1, an yeast ortholog of mammalian IP6K, exhibit defective endocytic trafficking and a fragmented vacuolar morphology, it has been speculated that 5-IP_7 and IP6K1 play a role in controlling endocytosis. However, the physiological actions of 5-IP_7 metabolism for the control of endocytic events in mammals have remained unanswered. Here, we demonstrate that endocytosis of synaptic vesicles at central synapses is markedly impaired in the hippocampus upon IP6K1 deletion (Figures 4 and 5), establishing IP6K and its product, 5-IP_7, as key physiological regulators of endocytic membrane trafficking events from yeast to mammals. With diminished synaptic vesicle reuse after vesicle exhaustion, IP6K1-KO hippocampal neurons exhibited a striking absence of sensitivity to the vacuolar ATPase inhibitor, folimycin, and dynamin inhibitor, dynasore, indicating that 5-IP_7 metabolism is essential for proper presynaptic vesicle endocytosis.

How might IP6K1 deletion influence synaptic endocytosis during exocytosis? Our current observations bear a remarkable resemblance to studies using dynamin 1-deficient animals (Ferguson et al., 2007; Hayashi et al., 2008). Cortical synapses obtained from dynamin 1-deleted mice exhibit impaired, activity-dependent synaptic vesicle recycling largely owing to incomplete endocytosis during activity (Ferguson et al., 2007; Hayashi et al., 2008). In support of this idea, in pancreatic beta cells, the 5-IP_7 precursor, IP_6, was found to control protein kinase C intracellular signaling cascades to drive the formation of phosphatidylinositol 4,5-bisphosphate ($PI(4,5)P_2$), a key lipid metabolite that triggers formation of clathrin-coated pits (Hoy et al., 2002). In addition to direct binding to target proteins, 5-IP_7 may also modulate protein functions by conferring a posttranslational modification known as pyrophosphorylation, which involves the transfer of a high-energy β-phosphate from 5-IP_7 to specific proteins (e.g., AP3 beta subunit, dynein intermediate chain) (Azevedo et al., 2009; Chanduri et al., 2016; Park et al., 2018). Identification of 5-IP_7-binding and pyrophosphorylation targets in the presynaptic terminal awaits further investigation.

Pharmacological blockade of dynamin phosphorylation by GSK3 impairs synaptic vesicle endocytosis in hippocampal synapses (Clayton et al., 2010). Thus, decreased GSK3 signaling in IP6K1-KO mice may partially mimic the blockade of dynamin phosphorylation and could thus account for the observed

impairment in endocytosis after excessive challenge (Figure 4). We should also consider competition between the IP6K1 catalytic product, 5-IP_7, and $PI(4,5)P_2$. Given that AP2 and AP180 are ligands for 5-IP_7 that bind with sub-nanomolar affinities (Norris et al., 1995; Voglmaier et al., 1992; Ye et al., 1995), the interplay among 5-IP_7, clathrin adaptor proteins, and plasma membrane phosphoinositides (e.g., $PI(4,5)P_2$) might be another route to endocytic regulation. The direct binding of GRAB to Rab11, a player in the control of activity-dependent bulk endocytosis (Horgan et al., 2013; Kokotos et al., 2019), further implies complex regulation of presynaptic vesicle trafficking by IP6K1-GRAB-Rab signaling cascades.

In conclusion, our findings unveil the physiological significance of the mammalian 5-IP_7 biosynthesis metabolism in controlling presynaptic vesicle cycling involving both exocytic and endocytic trafficking. Dysregulated IP metabolism in humans and genetic deletion of IP6K enzymes in mice have been linked to numerous psychiatric and neural diseases (Belmaker et al., 1996; Chakraborty et al., 2014; Nagata et al., 2011). Our next challenge will be to not only elucidate the molecular details of how IP6K1 and 5-IP_7 dynamically fine-tune synaptic vesicle exocytosis-endocytosis but also develop therapeutic strategies for controlling the release of neurotransmitters at central synapses.

Limitations of the Study

The expression of catalytically inactive mutant form of IP6K1 in *Ip6k1*-KO hippocampal neurons showed partial rescue of the *Ip6k1*-KO phenotypes, clearly suggesting that IP6K1 plays both 5-IP_7-dependent and 5-IP_7-independent functions at the central synaptic vesicle cycling events. Further works will be needed to validate IP6K1's non-catalytic actions. Additional experiments are also necessary to reveal the exact site and mode of IP6K1 action in the control of synaptic vesicle endocytosis.

METHODS

All methods can be found in the accompanying Transparent Methods supplemental file.

SUPPLEMENTAL INFORMATION

Supplemental Information can be found online at https://doi.org/10.1016/j.isci.2020.101000.

ACKNOWLEDGMENTS

We thank Dr. Jina Park and all the members of the Kim and Chung labs as well as Ms. Seung Min Park for discussion and helpful comments. This work was supported by the National Research Foundation of Korea (NRF-2013M3C7A1056102, NRF-2018R1A5A1024261, NRF-2018R1A2B2005913 to S.K.; NRF-2017R1A2B4006535, NRF-2015M3C7A1031395 to C.C.), TJ Park Science Fellowship of the POSCO TJ Park Foundation (to S.E.P.), and KAIST Advanced Institute for Science-X fellowship (to S.J.P.).

AUTHOR CONTRIBUTIONS

S.J.P., H.P., S.K., and C.C. conceived and designed the experiments. S.J.P., H.P., M.G.K., S.Z., and S.E.P. performed the experiments. S.J.P., H.P., S.K., and C.C. analyzed the data and co-wrote the paper. All authors discussed the results and commented on the manuscript.

DECLARATION OF INTERESTS

The authors declare no competing interests.

Received: June 7, 2019
Revised: February 17, 2020
Accepted: March 18, 2020
Published: April 24, 2020

REFERENCES

Azevedo, C., Burton, A., Ruiz-Mateos, E., Marsh, M., and Saiardi, A. (2009). Inositol pyrophosphate mediated pyrophosphorylation of AP3B1 regulates HIV-1 Gag release. Proc. Natl. Acad. Sci. U S A *106*, 21161–21166.

Belmaker, R.H., Bersudsky, Y., Agam, G., Levine, J., and Kofman, O. (1996). How does lithium work on manic depression? Clinical and psychological correlates of the inositol theory. Annu. Rev. Med. *47*, 47–56.

Chakraborty, A., Koldobskiy, M.a, Bello, N.T., Maxwell, M., Potter, J.J., Juluri, K.R., Maag, D., Kim, S., Huang, A.S., Dailey, M.J., et al. (2010). Inositol pyrophosphates inhibit Akt signaling, thereby regulating

insulin sensitivity and weight gain. Cell *143*, 897–910.

Chakraborty, A., Kim, S., and Snyder, S.H. (2011). Inositol pyrophosphates as mammalian cell signals. Sci. Signal. *4*, re1.

Chakraborty, A., Latapy, C., Xu, J., Snyder, S.H., and Beaulieu, J.-M. (2014). Inositol hexakisphosphate kinase-1 regulates behavioral responses via GSK3 signaling pathways. Mol. Psychiatry *19*, 284–293.

Chanduri, M., Rai, A., Malla, A.B., Wu, M., Fiedler, D., Mallik, R., and Bhandari, R. (2016). Inositol hexakisphosphate kinase 1 (IP6K1) activity is required for cytoplasmic dynein-driven transport. Biochem. J. *473*, 3031–3047.

Clayton, E.L., Sue, N., Smillie, K.J., O'Leary, T., Bache, N., Cheung, G., Cole, A.R., Wyllie, D.J., Sutherland, C., Robinson, P.J., et al. (2010). Dynamin I phosphorylation by GSK3 controls activity-dependent bulk endocytosis of synaptic vesicles. Nat. Neurosci. *13*, 845–851.

Doussau, F., Clabecq, A., Henry, J., Francois, D., and Poulain, B. (1998). Calcium-dependent regulation of Rab3 in short-term plasticity. J. Neurosci. *18*, 3147–3157.

Ertunc, M., Sara, Y., Chung, C., Atasoy, D., Virmani, T., and Kavalali, E.T. (2007). Fast synaptic vesicle reuse slows the rate of synaptic depression in the CA1 region of hippocampus. J. Neurosci. *27*, 341–354.

Fà, M., Staniszewski, A., Saeed, F., Francis, Y.I., and Arancio, O. (2014). Dynamin 1 is required for memory formation. PLoS One *9*, e91954.

Ferguson, S.M., Brasnjo, G., Hayashi, M., Wölfel, M., Collesi, C., Giovedi, S., Raimondi, A., Gong, L., Ariel, P., Paradise, S., et al. (2007). A selective activity-dependent requirement for dynamin 1 in synaptic vesicle endocytosis. Science *316*, 570–574.

Fernandez-Chacon, R., Konigstorfer, A., Gerber, S.H., Garcia, J., Matos, M.F., Stevens, C.F., Brose, N., Rizo, J., Rosenmund, C., and Sudhof, T.C. (2001). Synaptotagmin I functions as a calcium regulator of release probability. Nature *233*, 41–49.

Fu, C., Xu, J., Cheng, W., Rojas, T., Chin, A.C., Snowman, A.M., Harraz, M.M., and Snyder, S.H. (2017). Neuronal migration is mediated by inositol hexakisphosphate kinase 1 via α-actinin and focal adhesion kinase. Proc. Natl. Acad. Sci. U S A *114*, 2036–2041.

Geppert, M., Goda, Y., Hammer, R.E., Li, C., Rosahl, T.W., Stevens, C.F., and Sudhof, T.C. (1994). Synaptotagmin I: a major Ca2+ sensor for transmitter release at a central synapse. Cell *79*, 19717–19727.

Geppert, M., Goda, Y., Stevens, C.F., and Sudhof, T.C. (1997). The small GTP-binding protein Rab3A regulates a late step in synaptic vesicle fusion. Nature *387*, 810–814.

Guo, Z., Hou, X., Goody, R.S., and Itzen, A. (2013). Intermediates in the guanine nucleotide exchange reaction of Rab8 protein catalyzed by guanine nucleotide exchange factors Rabin8 and GRAB. J. Biol. Chem. *288*, 32466–32474.

Hatch, A.J., and York, J.D. (2010). SnapShot: inositol phosphates. Cell *143*, 1030–1030.e1.

Hayashi, M., Raimondi, A., O'Toole, E., Paradise, S., Collesi, C., Cremona, O., Ferguson, S.M., and De Camilli, P. (2008). Cell- and stimulus-dependent heterogeneity of synaptic vesicle endocytic recycling mechanisms revealed by studies of dynamin 1-null neurons. Proc. Natl. Acad. Sci. U S A *105*, 2175–2180.

Hilton, J.M., Plomann, M., Ritter, B., Modregger, J., Freeman, H.N., Falck, J.R., Krishna, U.M., and Tobin, A.B. (2001). Phosphorylation of a synaptic vesicle-associated protein by an inositol hexakisphosphate-regulated protein kinase. J. Biol. Chem. *276*, 16341–16347.

Horgan, C.P., Hanscom, S.R., and Mccaffrey, M.W. (2013). GRAB is a binding partner for the Rab11a and Rab11b GTPases. Biochem.Biophys. Res. Commun. *441*, 214–219.

Hoy, M., Efanov, A.M., Bertorello, A.M., Zaitsev, S.V., Olsen, H.L., Bokvist, K., Leibiger, B., Leibiger, I.B., Zwiller, J., Berggren, P.-O., et al. (2002). Inositol hexakisphosphate promotes dynamin I-mediated endocytosis. Proc. Natl. Acad. Sci. U S A *99*, 6773–6777.

Irvine, R.F., and Schell, M.J. (2001). Back in the water: the return of the inositol phosphates. Nat. Rev. Mol. Cell Biol. *2*, 327–338.

Kokotos, A.C., Peltier, J., Davenport, E.C., Trost, M., and Cousin, M.A. (2019). Activity-dependent bulk endocytosis proteome reveals a key presynaptic role for the monomeric GTPase Rab11. Proc. Natl. Acad. Sci. U S A *116*, 2386–2388.

Lee, T.-S., Lee, J.-Y., Kyung, J.W., Yang, Y., Park, S.J., Lee, S., Pavlovic, I., Kong, B., Jho, Y.S., Jessen, H.J., et al. (2016). Inositol pyrophosphates inhibit synaptotagmin-dependent exocytosis. Proc. Natl. Acad. Sci. U S A *113*, 8314–8319.

Llinás, R., Sugimori, M., Lang, E.J., Morita, M., Fukuda, M., Niinobe, M., and Mikoshiba, K. (1994). The inositol high-polyphosphate series blocks synaptic transmission by preventing vesicular fusion: a squid giant synapse study. Proc. Natl. Acad. Sci. U S A *91*, 12990–12993.

Lou, X., Fan, F., Messa, M., Raimondi, A., Wu, Y., Looger, L.L., and Ferguson, S.M. (2012). Reduced release probability prevents vesicle depletion and transmission failure at dynamin mutant synapses. Proc. Natl. Acad. Sci. U S A *109*, 515–523.

Luo, H.R., Saiardi, A., Nagata, E., Ye, K., Yu, H., Jung, T.S., Luo, X., Jain, S., Sawa, A., and Snyder, S.H. (2001). GRAB: a physiologic guanine nucleotide exchange factor for Rab3A , which interacts with inositol hexakisphosphate kinase. Neuron *31*, 439–451.

Macia, E., Ehrlich, M., Massol, R., Boucrot, E., Brunner, C., and Kirchhausen, T. (2006). Dynasore, a cell-permeable inhibitor of dynamin. Dev. Cell *10*, 839–850.

Nagata, E., Saiardi, A., Tsukamoto, H., Okada, Y., Itoh, Y., Satoh, T., Itoh, J., Margolis, R.L., Takizawa, S., Sawa, A., et al. (2011). Inositol hexakisphosphate kinases induce cell death in Huntington disease. J. Biol. Chem. *286*, 26680–26686.

Newton, A.J., Kirchhausen, T., and Murthy, V.N. (2006). Inhibition of dynamin completely blocks compensatory synaptic vesicle endocytosis. Proc. Natl. Acad. Sci. U S A *103*, 17955–17960.

Norris, F.A., Ungewickell, E., and Majerus, P.W. (1995). Inositol hexakisphosphate binds to clathrin assembly protein 3 (AP- 3/AP180) and inhibits clathrin cage assembly in vitro. J. Biol. Chem. *270*, 214–217.

Park, S.J., Lee, S., Park, S.E., and Kim, S. (2018). Inositol pyrophosphates as multifaceted metabolites in the regulation of mammalian signaling networks. Anim. Cells Syst. *22*, 1–6.

Rizo, J., and Rosenmund, C. (2008). Synaptic vesicle fusion. Nat. Struct. Mol. Biol. *15*, 665–674.

Saiardi, A., Erdjument-Bromage, H., Snowman, A.M., Tempst, P., and Snyder, S.H. (1999). Synthesis of diphosphoinositolpentakisphosphate by a newly identified family of higher inositol polyphosphate kinases. Curr. Biol. *9*, 1323–1326.

Saiardi, A., Sciambi, C., McCaffery, J.M., Wendland, B., and Snyder, S.H. (2002). Inositol pyrophosphates regulate endocytic trafficking. Proc. Natl. Acad. Sci. U S A *99*, 14206–14211.

Sankaranarayanan, S., and Ryan, T.A. (2001). Calcium accelerates endocytosis of vSNAREs at hippocampal synapses. Nat. Neurosci. *4*, 129–136.

Schluter, O.M., Basu, J., Sudhof, T.C., and Rosenmund, C. (2006). Rab3 superprimes synaptic vesicles for release: Implications for short-term synaptic plasticity. J. Neurosci. *26*, 1239–1246.

Schweizer, F.E., and Ryan, T.A. (2006). The synaptic vesicle: cycle of exocytosis and endocytosis. Curr.Opin.Neurobiol. *16*, 298–304.

Seeds, A.M., Frederick, J.P., Tsui, M.M.K., and York, J.D. (2007). Roles for inositol polyphosphate kinases in the regulation of nuclear processes and developmental biology. Adv. Enzyme Regul. *47*, 10–25.

Shears, S.B. (2015). Inositol pyrophosphates: why so many phosphates? Adv. Biol. Regul. *57*, 203–216.

Südhof, T.C. (2004). The synaptic vesicle cycle. Annu. Rev. Neurosci. *27*, 509–547.

Thanawala, M.S., and Regehr, W.G. (2013). Presynaptic calcium influx controls neurotransmitter release in part by regulating the effective size of the readily releasable pool. J. Neurosci. *33*, 4625–4633.

Voglmaier, S.M., Keen, J.H., Murphy, J.E., Ferris, C.D., Prestwich, G.D., Snyder, S.H., and Theibert, A.B. (1992). Inositol hexakisphosphate receptor identified as the clathrin assembly protein AP-2. Biochem.Biophys. Res. Commun. *187*, 158–163.

Wenk, M.R., and De Camilli, P. (2004). Protein-lipid interactions and phosphoinositide metabolism in membrane traffic: Insights from

vesicle recycling in nerve terminals. Proc. Natl. Acad. Sci. U S A *101*, 8262–8269.

Wilson, M.S.C., Livermore, T.M., and Saiardi, A. (2013). Inositol pyrophosphates: between signalling and metabolism. Biochem. J. *452*, 369–379.

Yang, S.-N., Shi, Y., Yang, G., Li, Y., Yu, L., Shin, O.-H., Bacaj, T., Südhof, T.C., Yu, J., and Berggren, P.-O. (2012). Inositol hexakisphosphate suppresses excitatory neurotransmission via synaptotagmin-1 C2B domain in the hippocampal neuron. Proc. Natl. Acad. Sci. U S A *109*, 12183–12188.

Ye, W., Ali, N., Bembenek, M.E., Shears, S.B., and Lafer, E.M. (1995). Inhibition of clathrin assembly by high affinity binding of specific inositol polyphosphates to the synapse-specific clathrin assembly protein AP-3. J. Biol. Chem. *270*, 1564–1568.

iScience, Volume *23*

Supplemental Information

Inositol Pyrophosphate Metabolism Regulates Presynaptic Vesicle Cycling at Central Synapses

Seung Ju Park, Hoyong Park, Min-Gyu Kim, Seungjae Zhang, Seung Eun Park, Seyun Kim, and ChiHye Chung

SUPPLEMENTAL FIGURES

Figure S1

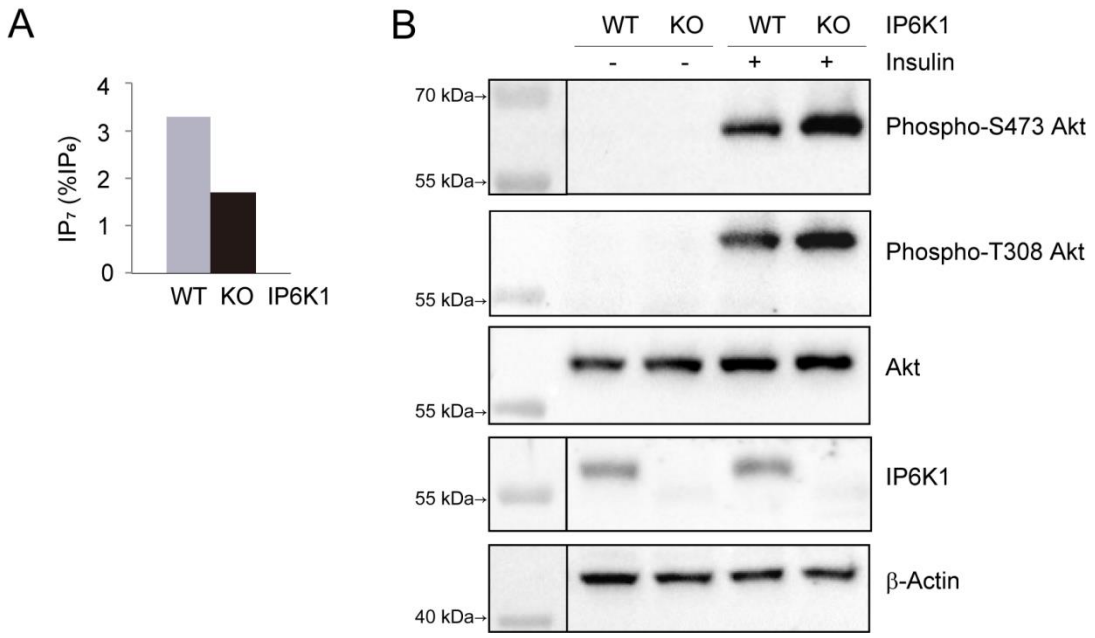

Supplemental Figure S1, related to Figure 1. Analysis of IP_7 level and Akt signaling in primary hepatocytes of IP6K1-KO mice.

(A) WT and IP6K1-KO primary hepatocytes were isolated from mice and labeled with 60 μCi [^{3}H]-myo-inositol (PerkinElmer) in DMEM medium for 3 days. HPLC analysis of ^{3}H-labeled IP contents were measured by scintillation counter. The level of IP_7 was decreased about 50% in KO cells. (B) WT and IP6K1-KO primary hepatocytes were stimulated with insulin for 15 min. Immunoblot analysis of phosphorylated Akt showed that Akt activity was increased in IP6K1-KO hepatocytes. These findings are similar to those previously reported (Chakraborty et al., 2010), confirming the successful generation of IP6K1-KO mice by targeting the ATG codon of *Ip6k1* exon 2 using the CRISPR/Cas9 system. Unrelated intervening lanes from the same Immunoblots were cropped. Solid lines are for readability only.

Figure S2

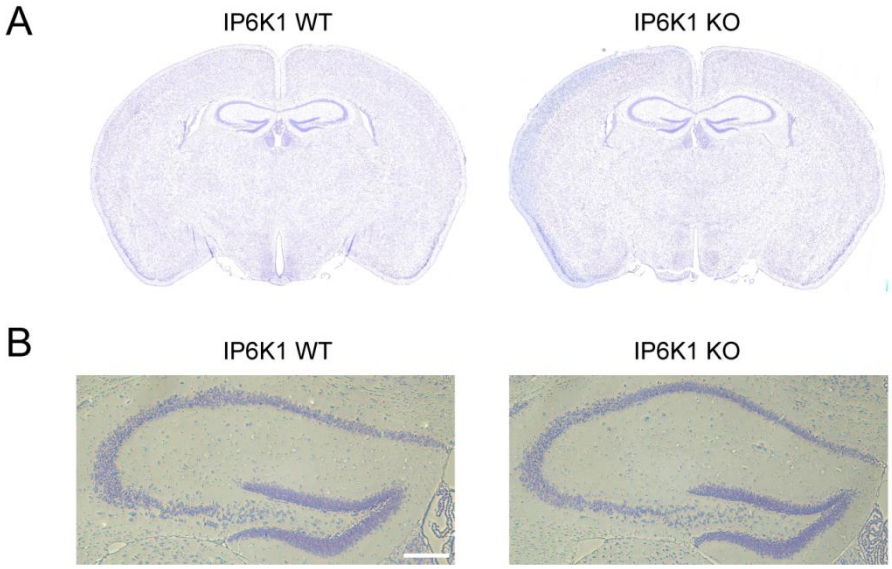

Supplemental Figure S2, related to Figure 1. Characterization of the adult IP6K1-KO brain.

Nissl staining showed normal brain structures in adult (8-week-old) IP6K1-KO mice. (A) Representative images of hippocampal regions (B). Scale bar, 1 mm.

Figure S3

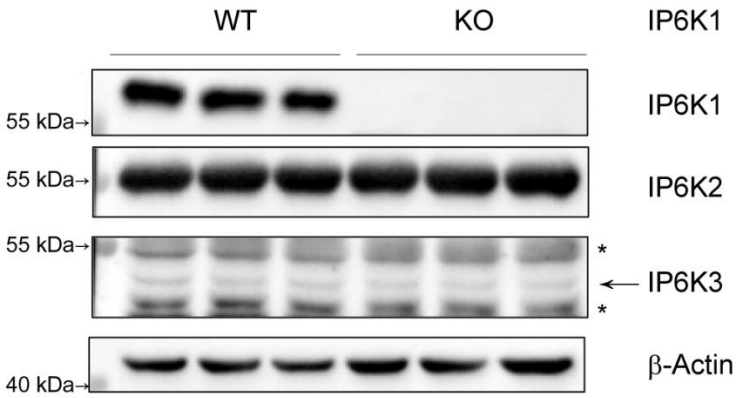

Supplemental Figure S3, related to Figure 1. Expression of IP6K1 isoforms in the hippocampus of IP6K1-KO mice.

Immunoblotting of IP6K2 and IP6K3 in hippocampi of WT and IP6K1-KO mice. The expression level of IP6K2 and IP6K3 was verified by immunoblotting in IP6K1 KO mouse hippocampus tissue lysate. The knockout of IP6K1 in mouse hippocampus did not affect the either IP6K2 or IP6K3 expression. Asterisks are non-specific bands.

Figure S4

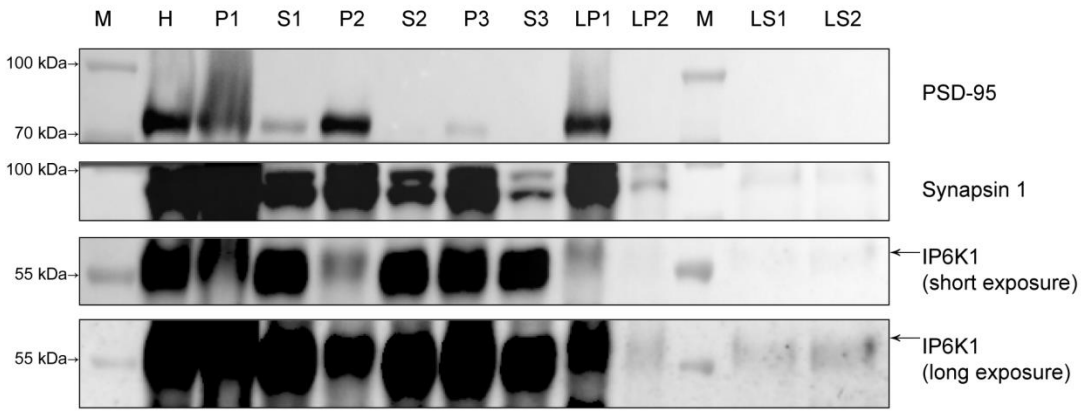

Supplemental Figure S4, related to Figure 1. Expression of IP6K1 in synaptic fractions.

Distribution of IP6K1 in subcellular fractionations of adult mouse brain (n=4). Synaptic marker protein PSD-95 was found in crude synaptosomal fraction (P2) and synaptosomal membrane fraction (LP1). Another presynaptic marker, Synapsin I was observed in every fractions, including LP2, LS1, and LS2. Similar to Synapsin I, IP6K1 was detected in LP1, LP2, LS1, and LS2 fraction (H, homogenates; P1, nucleus and other debris; P2, crude synaptosomal fraction; P3, light membranes and Golgi; S3, cytosol fraction; LP1, synaptosomal membrane fraction; LS1, cytosol contained in synaptosomes; LP2, synaptic vesicle enriched fraction; LS2, soluble fraction). M (lane 1 and 9) indicates protein size marker.

Figure S5

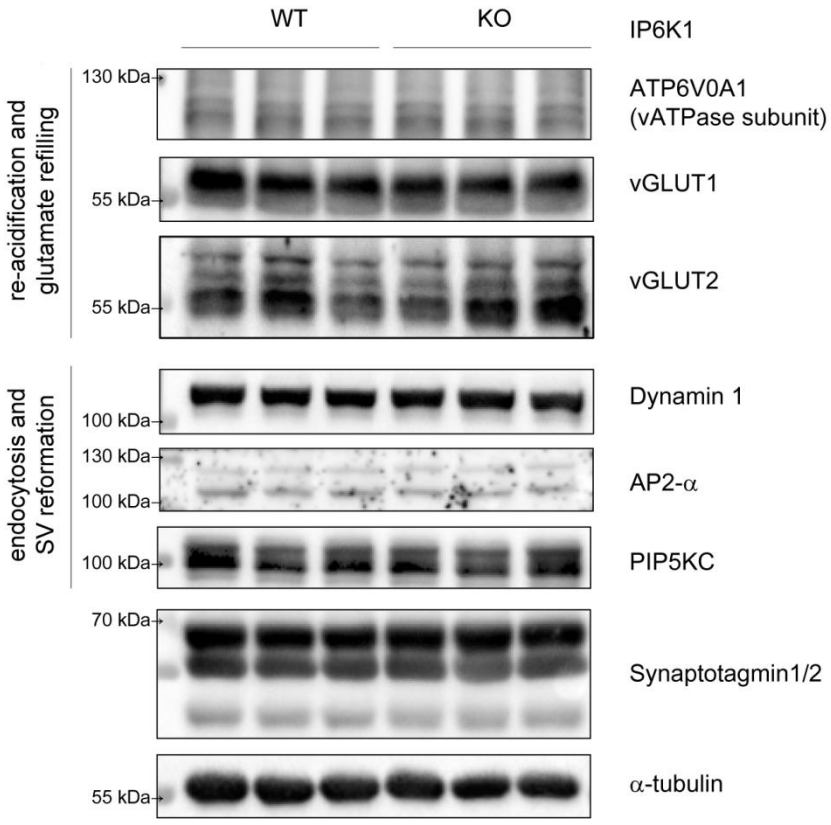

Supplemental Figure S5, related to Figure 1. Expression of synaptosomal proteins in the hippocampus of IP6K1-KO mice.

Immunoblotting of synaptosomal proteins in hippocampi of WT and IP6K1-KO mice. The knockout of IP6K1 in mouse hippocampus did not affect the expression levels of presynaptic proteins.

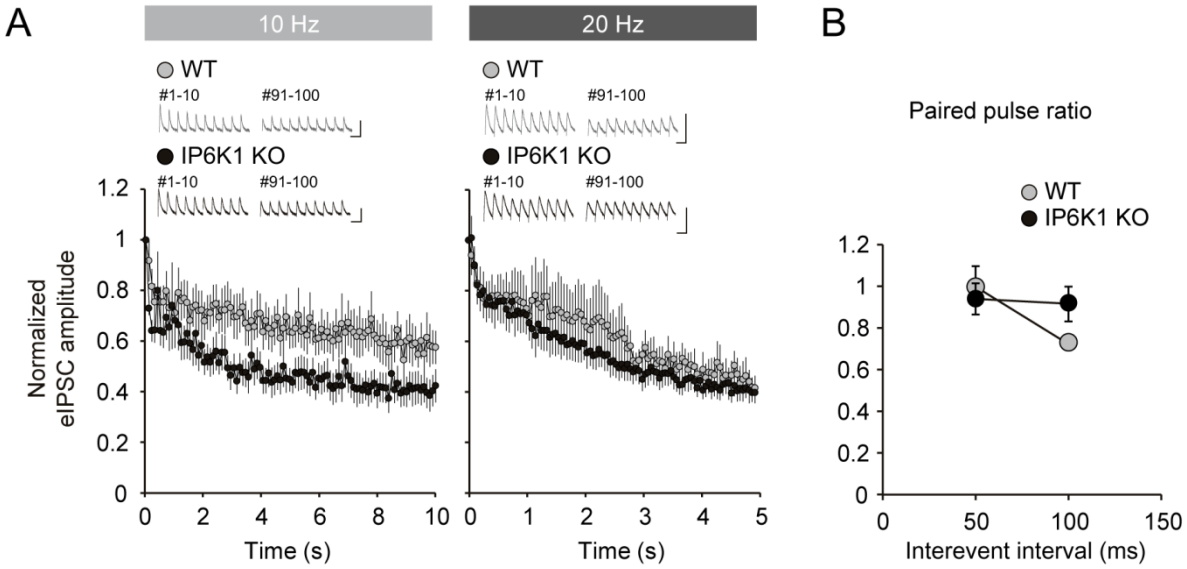

Supplemental Figure S6, related to Figure 2. Presynaptic release probability is not altered in hippocampal inhibitory synapses in IP6K1-KO mice.

(A) Normalized eIPSC amplitudes at various frequencies of stimulation were not different significantly between IP6K1-KO and WT mice at stimulation frequencies of 10 Hz (*$p < 0.05$ for 2-3, 23-52 and 75-80; n = 10–11) or 20 Hz (minimum $p > 0.18$; n = 10-11). Scale bars for representative traces: 100 pA and 100 ms. (B) PPR showed no activity-dependent difference (Two-way ANOVA analysis, $F_{(1,20)} = 0.67$, $p > 0.41$ for genotype; $F_{(1,20)} = 4.02$, $p > 0.05$ for frequency).

TRANSPARENT METHODS

STAR METHODS

KEY RESOURCES TABLE

REAGENT or RESOURCE	SOURCE	IDENTIFIER
Antibodies		
Rabbit anti-IP6K1	GeneTex	GTX103949
Mouse anti-GAPDH	Santa Cruz	Sc-32233
Rabbit anti-phospho-S473 Akt	Cell Signaling Technology	CST-9271
Rabbit anti-phospho-T308 Akt	Cell Signaling Technology	CST-4056
Rabbit anti-Akt	Cell Signaling Technology	CST-9272
Rabbit anti-β−actin	Cell Signaling Technology	CST-4970
Rabbit anti-Dynamin1	Invitrogen	PA1-660
Mouse anti-AP2 alpha	Thermo Fisher	MA1-064
Mouse anti-PSD95	Thermo Fisher	MA1-046
Rabbit anti-ATP6V0A1	Novus	NBP1-89342
Guinea Pig anti-vGLUT1	Millipore	AB5905
Guinea Pig anti-vGLUT2	Millipore	AB2251
Rabbit anti-synaptotagmin 1/2	MBL	D156-3
Rabbit anti PIP5KC	Abcam	Ab109192
Mouse anti-IP6K2	Santa Cruz	Sc-373770
Rabbit anti-IP6K3	Sigma Aldrich	SAB4500277
Rabbit anti-synapsin1	Merck	AB1543
IP6K1 Forward primer (GCCAGGATCAACTTAGCTCT)	Macrogen	N/A
IP6K1 Reverse primer (CATCTCCCGGGAACAGCGCT)	Macrogen	N/A

Chemicals, Peptides, and Recombinant Proteins		
[^{3}H]myo-inositol	Perkin Elmer	NET1177001MC
Tetrodotoxin citrate (Octahydro-12-(hydroxymethyl)-2-imino-5,9:7,10a-dimethano-10aH-[1,3]dioxocino[6,5-d]pyrimidine-4,7,10,11,12-pentol citrate)	Tocris Biosciences	1069
D-AP5 (D-(-)-2-Amino-5-phosphonopentanoic acid)	Tocris Biosciences	0106
Cyanquixaline (6-Cyano-7-nitroquinoxaline-2,3-dione)	Tocris Biosciences	0190
Folimycin (Concanamycin A)	Sigma Aldrich	C9705
Dynasore hydrate (N-[(E)-(3,4-dihydroxyphenyl)methylideneamino]-3-hydroxynaphthalene-2-carboxamide;hydrate)	Sigma Aldrich	D7693
Picrotoxin ((1R,3R,5S,8S,13R,14S)-1-hydroxy-14-(2-hydroxypropan-2-yl)-13-methyl-4,7,10-trioxapentacyclo[6.4.1.19,12.03,5.05,13]tetradecane-6,11-dione;(1R,5S,8S,13R,14R)-1-hydroxy-13-methyl-14-prop-1-en-2-yl-4,7,10-trioxapentacyclo[6.4.1.19,12.03,5.05,13]tetradecane-6,11-dione)	Sigma Aldrich	P1675
Papain	Worthington	LS003126
L-Cysteine	Sigma Aldrich	C7352

Poly-L-ornithine hydrobromide	Sigma Aldrich	P3655
Sodium tetraborate	Sigma Aldrich	221732
Boric acid	Sigma Aldrich	B9645
Neurobasal A	Gibco	10888022
B27	Invitrogen	A352801
penicillin/streptomycin	Invitrogen	15140-122
HBSS	Welgene	LB003-04
glucose	Sigma Aldrich	G7021
sucrose	Sigma Aldrich	S1888
Experimental Models: Organisms/Strains		
IP6K1-KO mice	Toolgen	N/A
Software and Algorithms		
Clampex 10.3	Molecular Devices	www.moleculardevices.com
WinLTP	Synaptic Electrophysiology Software	www.winltp.com
Mini Analysis software	Synaptosoft	http://www.synaptosoft.com

CONTACT FOR REAGENT AND RESOURCE SHARING

Further information and requests for resources and reagents should be directed to and will be fulfilled by the Lead Contacts, Seyun Kim (seyunkim@kaist.ac.kr) or ChiHye Chung (cchung@konkuk.ac.kr)

EXPERIMENTAL MODEL AND SUBJECT DETAILS

IP6K1-KO mice, generated by Toolgen, Inc. (Seoul, Korea), were interbred and maintained under pathogen-free conditions at Macrogen, Inc. (Seoul, Korea). All

manipulations were conducted with the approval of the Macrogen Institutional Animal Care and Use Committee. Two single-guide RNA (sgRNA) sequences targeting sites upstream (sgRNA1-TTTGTCAAACCATGGAAGTGGGG) and downstream (sgRNA2-CCGCCCACCTGATGGATGAAGGG) of exon 2 in the *Ip6k1* gene were transcribed in vitro. Prepared sgRNA (5 μg) and Cas9 protein (10 μg) were mixed with injection buffer (500 μl), and a mixture of sgRNA1, sgRNA2, and Cas9 protein was microinjected into one-cell embryos. After F0 mice harboring an out-of-frame, 73-bp deletion mutation were born, genotyping was performed using tail-snip samples and confirmed by T7 endonuclease 1 (M0302S; NEB) digestion and sequencing analysis. The genotyping primers are detailed below. IP6K1-F (5'-GCCAGGATCAACTTAGCTCT-3') anneals to a sequence upstream of the *Ip6k1* gene; IP6K1-R (5'-CATCTCCCGGGAACAGCGCT-3') anneals to a sequence downstream of the *Ip6k1* gene cluster. IP6K1-F and IP6K1-R amplify a fragment of 178 bp corresponding to the knockout allele and a fragment of 251 bp corresponding to the WT allele. Mice were maintained on a C57BL/6J background and kept in an enriched environment under standard conditions with a 12-h light/dark cycle. Animal studies were performed in accordance with the recommendations of the Guide for the Care and Use of Laboratory Animals of the National Institutes of Health. The protocol was approved by the Konkuk University Institutional Animal Care and Use Committee. Animal protocols, materials, and methods were performed in accordance with guidelines approved by the Institutional Review Board of the Korea Advanced Institute of Science and Technology Animal Care and Use Committee.

METHOD DETAILS

In vitro electrophysiology

All electrophysiological recordings were performed by researchers blinded to group-identifying information. Acute hippocampus-containing brain slices were prepared from 4–7-week-old male mice. For electrophysiology, brains were extracted from animals anesthetized with isoflurane, then placed in ice-cold dissection buffer (212 mM sucrose, 3 mM KCl, 26 mM $NaHCO_3$, 1.25 mM NaH_2PO_4, 7 mM $MgCl_2$, and 10 mM glucose), gassed with 95% O_2 and 5% CO_2. Coronal brain slices (~300–350 μm thick) containing the hippocampus were prepared using a vibratome (Leica VT 1000S). Brain slices were transferred to a recovery chamber filled with artificial cerebrospinal fluid (aCSF; 118 mM NaCl, 2.5 mM KCl, 11 mM glucose, 1 mM NaH_2PO_4, and 26.2 mM $NaHCO_3$), gassed with 95% O_2 and 5% CO_2, then incubated at 35°C for 1 h and stored at room temperature. Hippocampal CA1 neuronal activity was recorded in aCSF using an Axopatch 200B or Multiclamp 700B amplifier. Recorded signals were filtered at 2 kHz and sampled at 40 kHz (miniature synaptic transmission) or 20 kHz (evoked synaptic transmission) using Clampex 10.3 (Molecular Devices) or WinLTP (Synaptic Electrophysiology Software). For voltage-clamp analyses, glass pipettes with a resistance of 2–6 MΩ were filled with an internal solution consisting of 115 mM Cs-methanesulphonate, 20 mM CsCl, 10 mM HEPES, 2.5 mM $MgCl_2$, 0.6 mM EGTA, 5 mM QX314, 4 mM Na_2-ATP, 0.4 mM Na_2-GTP, and 10 mM Na-phosphocreatine (pH 7.3). Miniature excitatory synaptic transmissions (mEPSCs) were recorded at a holding potential of -60 mV. GABA receptor-mediated inhibitory synaptic transmission was excluded by performing mEPSC recordings in the presence of 1 μM tetrodotoxin (TTX) and 50 μM picrotoxin (PTX). Miniature inhibitory synaptic transmissions (mIPSCs) were recorded at a

holding potential of 0 mV in the presence of 1 μM TTX, 10 μM cyanquixaline (CNQX), and 50 μM AP5 to exclude glutamate receptor-mediated synaptic transmission. For recordings of evoked synaptic transmission, eEPSCs and eIPSCs were elicited by stimulating the Schaffer-collateral pathway (CA1 input from CA3) using platinum/Iridium cluster electrodes (FHC). eEPSCs were recorded at a holding potential of -60 mV in aCSF containing 50 μM PTX. eIPSCs were recorded at a holding potential of 0 mV in aCSF containing 10 μM CNQX and 50 μM AP5.

Generation of AAV-mIP6K1 viral particles

pAAV-IP6K1 viral particles were generated by Institute for Basic Science (IBS) virus facility. Mouse IP6K1 cNDA (NM_013785.2) was used for cloning. In brief, AAV-EGFP, AAV-IP6K1-WT, or AAV-IP6K1-K226A constructs were co-transfected with pSerotype2 and pHelper vector into 1×10^7 HEK293T cells plated in 150 mm dish. After 48 h, cells were harvested with lysis buffer added 50 U/ml Benzonase and incubated in 37°C for 30 min. 3 cycles of freeze and thaw were followed. The viral particles were then purified via ultracentrifugation and concentrated through 100 MWCO filter. The titration of viral particle was measured by quantitative PCR.

Stereotaxic surgery

4–5-week-old male IP6K1-KO mice were anaesthetized with isoflurane. 300nl of virus was bilaterally injected into hippocampal CA3 regions following coordinates from bregma: A/P, -2.4 mm; M/L, ±2.8 mm; D/V, -2.2 mm, using syringe and syringe pump (Chemyx Inc. injection flow rate : 0.08 μl/min). After surgery, mice were single-housed and allowed to expression of coded proteins for 4 weeks.

Subcellular fractionation

After anesthesia, the mouse brain tissues were quickly isolated. Brain tissues were ground into ice-cold homogenization buffer(0.32 M Sucrose, 4 mM HEPES, 1 mM $MgCl_2$, 0.5 mM $CaCl_2$, pH7.4 with freshly added protease inhibitors and 2 mM DTT). The homogenates were separated into pellet (P1) and supernatant (S1) through centrifuge for 10min at 1000 x g at 4°C. The pellet (P1) contains nuclei and large debris. The centrifugation of supernatant (S1) at 12000 x g for 15 min resulted in the crude synaptosomal fraction (P2), and supernatant (S2). S2 was further centrifuged at 25000 x g to obtain light membrane (P3) and cytosol fraction (S3). And then, the crude synaptosomal fraction (P2) fraction was dissolved by hypotonic lysis and centrifuged for 20 min at 33000 x g to yield synaptosomal membranes fraction (LP1). The remaining supernatant (LS1) was centrifuged at 250000 x g to deposit a crude synaptic vesicle-enriched fraction (LP2) and soluble fraction (LS2). (H, homogenates; P1, nucleus and other debris; P2, crude synaptosomal fraction; P3, light membranes and Golgi; S3, Cytosol fraction; LP1, synaptosomal membrane fraction; LS1, cytosol contained in synaptosomes; LP2, synaptic vesicle enriched fraction; LS2, soluble fraction)

Immunoblotting

Protein lysates of the hippocampus, cortex, and cerebellum were prepared from 8-week-old WT or IP6K1-KO mice. Tissues were homogenized in lysis buffer (1% NP-40, 137 mM NaCl, 20 mM Tris-HCl (pH 8.0), 2 mM EDTA, 10% glycerol, 20 mM Na_3VO_4, 10 mM sodium pyrophosphate, 100 mM sodium fluoride, 20 mM PMSF)

containing protease inhibitor cocktail (Roche). Generally, 20 μg of protein lysates were resolved by sodium dodecyl sulfate-polyacrylamide gel electrophoresis (SDS-PAGE) and blotted with primary antibodies and species-appropriate horseradish peroxidase (HRP)-conjugated secondary antibodies. HRP signals were visualized using Clarity ECL substrate (Bio-Rad) and measured using ChemiDoc (Bio-Rad). IP6K1 and GAPDH antibodies were from Genetex and Santa Cruz Biotechnology, respectively. Phospho-Akt, total Akt, and β-actin antibodies were purchased from Cell Signaling Technology. Virus injected hippocampal tissues were dissected from acute brain slices after electrophysiological recording for Western blot analysis.

Histology

Mice were transcardially perfused and sectioned. For cresyl violet staining, mouse brain sections were mounted onto gelatin-coated slides. Cresyl violet staining solutions contain as following: 0.1% cresyl violet acetate (Sigma) and glacial acetic acid (Georgia Chem). The slides were dipped continuously into cresyl violet staining solution (8 min, 60ºC), distilled water (3 min), 70% ethanol (3 min), 95% ethanol (2 min), 100% ethanol (1 min), and xylene (5 min). After dehydration, the sections were mounted with Canada Balsam (Kanto). Images were acquired using Axio Scan (Carl Zeiss).

Primary hippocampal neuron culture

Hippocampi were dissected out from brains of 17.5-day embryos of WT or IP6K1-KO mice, and placed in ice-cold Hanks' balanced salt solution (HBSS) with 28 mM glucose and 20 mM sucrose. Then, the tissues were incubated with 0.125% trypsin in HBSS solution for 15 min at 37°C, and disassociated by repeated passage

through a 10-ml disposable pipette. The cells were pelleted at 1650 rpm for 5 min, and resuspended in neurobasal medium supplemented with B-27, 2 mM L-glutamine and 1% penicillin/streptomycin. Neurons were seeded at 8 × 10^5 cells onto 6-well plates coated with poly-L-ornithine (100 μg/ml) in borate buffered system, and maintained in a humidified 5% CO_2 incubator at 37°C for 13 days. Half of the medium was exchanged with fresh medium every 3 days. 9 days after culture, cells were labeled with [^{3}H]-myo-inositol for measuring IP content.

HPLC analysis of intracellular IP content

Primary hippocampal neurons and hepatocytes were isolated from mice were labeled with 60 μCi [^{3}H]-myo-inositol (PerkinElmer) in Neurobasal A/B27 or DMEM medium respectively for 3 days. Soluble IPs were extracted from labeled cells as described (Lee et al., 2016). Inositol incorporated into lipids was measured by extracting the remaining cell pellet with 0.1 M NaOH and 0.1% Triton X-100 for 12 h at room temperature with shaking, and counting a fraction of the solubilized material in a liquid scintillation counter. Soluble IP levels were normalized to total lipid inositol content. ^{3}H-labeled IPs were resolved by high-performance liquid chromatography (HPLC), as described previously (Lee et al., 2016).

Data Analysis

Data were analyzed using Clampfit 10.3 (Molecular Devices), Mini Analysis software (Synaptosoft), and WinLTP (Synaptic Electrophysiology Software). Evoked synaptic transmissions were normalized to average peak amplitude before drug application for at least 5 min. PPRs were measured as the ratio of the 2nd peak amplitude to the

1st peak amplitude. Total RRP size was estimated by using linear extrapolation from cumulative eEPSC charge transfer curves. Release probability was calculated by 1st eEPSC charge transfer divided by total charge transfer during 20 Hz for 100 times. Decay time constants (during 20 Hz stimulation) and rise time constants (during 1 Hz stimulation) were calculated by fitting the normalized eEPSCs amplitude with a single exponential function starting at the peak amplitude. The equations, $f(x) = a\ \{1 - \exp(-x/\tau)\} + 1$ and $f(x) = -\ b\ \{1 - \exp(-x/\tau)\}$were used for calculating the decay time constant and rise time constant, respectively. The values are given as means ± SEM, and two-tailed unpaired t-tests were used for statistical comparisons unless stated otherwise.

SUPPLEMENTAL REFERENCES

Chakraborty, A., Koldobskiy, M. a, Bello, N.T., Maxwell, M., Potter, J.J., Juluri, K.R., Maag, D., Kim, S., Huang, A.S., Dailey, M.J., et al. (2010). Inositol pyrophosphates inhibit Akt signaling, thereby regulating insulin sensitivity and weight gain. Cell *143*, 897–910.

Lee, T.-S., Lee, J.-Y., Kyung, J.W., Yang, Y., Park, S.J., Lee, S., Pavlovic, I., Kong, B., Jho, Y.S., Jessen, H.J., et al. (2016). Inositol pyrophosphates inhibit synaptotagmin-dependent exocytosis. Proc. Natl. Acad. Sci. *113*, 8314–8319.